IEEE Access
Multidisciplinary ⋮ Rapid Review ⋮ Open Access Journal

Received 20 February 2024, accepted 19 March 2024, date of publication 29 March 2024, date of current version 4 April 2024.

Digital Object Identifier 10.1109/ACCESS.2024.3383161

RESEARCH ARTICLE

Performance and Cost Comparison of Drive Technologies for a Linear Electric Machine Gravity Energy Storage System

MORRIS MUGYEMA[1], (Graduate Student Member, IEEE), MAARTEN J. KAMPER[1], (Senior Member, IEEE), RONG-JIE WANG[1], (Senior Member, IEEE), AND BEN A. SEBITOSI[2], (Senior Member, IEEE)

[1]Department of Electrical and Electronic Engineering, Stellenbosch University, Stellenbosch 7602, South Africa
[2]Department of Mechanical and Mechatronic Engineering, Stellenbosch University, Stellenbosch 7602, South Africa

Corresponding author: Morris Mugyema (25704656@sun.ac.za)

This work was supported by the Center for Renewable and Sustainable Energy Studies (CRSES), Stellenbosch University as part of the Mobility of African Scholars for Transformative Engineering Training (MASTET).

ABSTRACT Energy storage is a crucial technology for facilitating the integration of renewable energy sources (RES), such as wind and solar energy, into the electrical grid. The challenge of maintaining a balance between incoming and outgoing grid power can be effectively addressed by integrating energy storage technologies with inherently intermittent RES. A range of viable options for storing energy from RES currently exists, among which the Linear Electric Machine Gravity Energy Storage System (LEM-GESS) stands out as a promising choice. The LEM-GESS stores energy in a shaft using piston masses based on the concept of gravity. This paper presents the performance and cost analysis of different linear machines employed as the main drive units in a dry gravity energy storage system. Specifically, linear permanent magnet flux switching machine demonstrates the best performance in terms of overall system cost when considering a 20 MW/10 MWh system and optimizing for the minimum levelized cost of storage (LCOS). Noteworthy findings reveal that the LEM-GESS cost is highly sensitive to system efficiency, with factors such as material cost and power factor also influencing the LCOS. Designs with modest secondary height, low usage of copper and magnet materials on the primary of the LEM, and a high power factor are preferred to minimize the LCOS. In conclusion, the LEM-GESS with a permanent magnet machine drive option is a highly promising and cost-effective technology for supporting the integration of RES into the grid.

INDEX TERMS Dry gravity, energy storage, levelized cost of storage, linear machine, optimization, renewable energy sources.

NOMENCLATURE

Symbols

h	Shaft height.
w_p	Piston width.
l_p	Piston height.
A	Air gap area.
a	Acceleration.
m	Mass.
g	Gravitational constant.
τ_t	Secondary tooth pitch.
n	Integer.
n_s	Number of secondary teeth.
p_{pm}	PM pole pairs.
p_a	Armature winding pole pairs.
v_ϕ	Speed of the magnetic field.
v_t	Speed of the primary.
G_r	Gear ratio.
J	Current density.

The associate editor coordinating the review of this manuscript and approving it for publication was Alfeu J. Sguarezi Filho.

h_{my}	Primary mover yoke height.
h_{mt}	Primary mover tooth height.
w_{mt}	Width of mover tooth.
w_{ms}	Width of mover slot.
w_{pm}	Width of PM.
w_{fw}	Width of field winding.
h_{fw}	Height of field winding.
w_{st}	Width of secondary tooth.
h_{st}	Height of secondary tooth.
h_{sc}	Height of secondary core.
d_s	Mover displacement.
P_{out}	Output power.
P_{cu}	Copper losses.
P_{iron}	Iron losses.
E_o	Induced voltage.
V_o	Terminal voltage.
I_q	q-axis current.
I_d	d-axis current.
X_q	Synchronous reactance.
σ	Shear stress.
ρ	Density.
\$	Dollar.
η	Efficiency.

Abbreviations

AC	Alternating Current.
CAPEX	Capital Expenditure.
CIR	Circumferential.
CP-LVHM	Consequent Pole Linear Vernier Hybrid Machine.
DC	Direct Current.
EMF	Electromagnetic Force.
FEA	Finite Element Analysis.
GW	Gigawatt.
LCOS	Levelized Cost of Storage.
LEM-GESS	Linear Electric Machine Gravity Energy Storage System.
LPM-FSM	Linear Permanent Magnet Flux Switching Machine.
LWF-FSM	Linear Wound Field Flux Switching Machine.
MMF	Magnetomotive Force.
MW	Megawatt.
MWh	Megawatt-hour.
NSGA	Non-dominated Sorting Genetic Algorithm.
OPEX	Operation Expenditure.
PM	Permanent Magnet.
RES	Renewable Energy Sources.
TOR	Toroidal.

I. INTRODUCTION

The substantial rise in the world's energy consumption can be attributed to rapid industrialization and economic expansion, particularly in developing nations [1]. Fossil fuels currently constitute approximately 80% of the global energy mix, underscoring their predominant reliance on non-renewable resources [2].

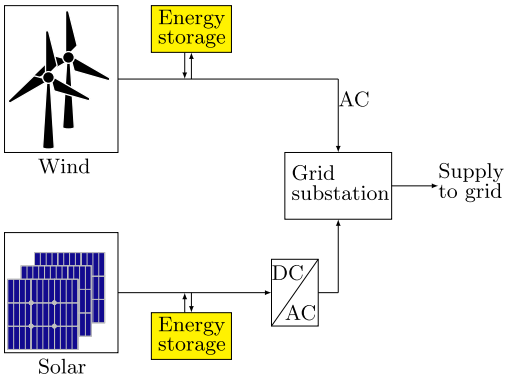

FIGURE 1. RES connected to the grid with energy storage.

In response to the escalating environmental concerns posed by the substantial carbon dioxide emissions associated with fossil fuel consumption, there has been a concerted effort to transition towards Renewable Energy Sources (RES) [3]. This strategic shift aims to alleviate environmental impacts by curbing the extensive demand for fossil fuels. The overarching goal is to align with the targets set in the Paris Agreement, which emphasizes the imperative of limiting the average global temperature increase to well below 2° C [4]. Consequently, the deployment of RES serves as a crucial means to address both environmental and climate challenges intertwined with the prevailing energy demand.

In 2023, there was a remarkable surge in global annual renewable capacity addition, marking impressive growth of almost 50%, reaching nearly 510 gigawatts (GW) [5]. This growth rate has been the fastest observed over the past two decades, with China leading the way by commissioning the highest capacity.

According to the International Energy Agency (IEA), projections for the 2023-2028 period indicate an extraordinary addition of almost 3 700 GW in new renewable capacity, primarily propelled by supportive policies on a global scale. This surge in capacity expansion signifies a monumental shift towards cleaner and more sustainable energy sources. Notably, solar photovoltaic and wind energy are set to play pivotal roles, accounting for a staggering 95% of the overall global renewable expansion [5]. This dominance is fueled by their competitive advantage in terms of lower generation costs compared with both fossil and non-fossil fuel alternatives. The collective impact of these developments shows a significant stride towards a more sustainable and environmentally conscious global energy landscape.

Nevertheless, the seamless integration of RES, such as wind and solar energy, into the global energy landscape faces challenges primarily stemming from their intermittent nature [6]. The inherent stochastic characteristics of these renewable sources introduce operational and control uncertainties into the grid. This unpredictability poses a significant impediment to the widespread adoption of RES

on the grid. The uncertainty associated with renewable energy generation underscores the need for a resilient and adaptable network to effectively manage the balance between supply and demand [7].

To address this challenge, energy storage systems have emerged as promising solutions to mitigate the effects of intermittency and enhance the overall flexibility and stability of the grid [8]. Fig. 1 shows the connection between the RES and energy storage systems to the power grid. Through their capability to absorb or discharge energy as required, energy storage systems provide essential grid support. This pivotal role not only addresses the uncertainties introduced by renewable sources but also contributes significantly to the increased integration of renewable energy into the power grid [9]. RES can benefit from energy storage systems and potentially become a reliable primary source of energy.

The recently proposed linear electric machine gravity energy storage system (LEM-GESS) operates based on the principle of gravity, utilizing dry object masses to store electrical energy as potential energy at a given height h [10]. This innovative system, which has a potentially long lifespan, high charge-discharge capability, high thrust and low speed characteristics, has been thoroughly examined in [11]. The analysis revealed that the LEM-GESS exhibits economic feasibility, particularly in primary response application.

Primary response entails the correction of frequency fluctuations within the power network [12]. In [13], the LEM-GESS was subjected to a comparative analysis with other energy storage systems used for primary response, namely, lithium-ion, vanadium, lead acid, and flywheel energy storage systems.

The findings of the comparison indicate that the LEM-GESS with Δh of 1000 m is remarkably competitive. Its performance and cost-effectiveness make it a promising and viable alternative for primary response application, highlighting its potential to address the challenges associated with frequency fluctuations in power networks.

However, it is crucial to highlight that the selection of the linear electric machine utilized as the main drive unit for the LEM-GESS significantly influences the overall performance of this technology. Machine-related factors such as efficiency, power factor, and material composition, play pivotal roles in determining the economic viability of the entire LEM-GESS. Therefore, it is necessary to conduct a thorough analysis of various machine technologies with the aim of enhancing both the performance and cost-effectiveness of the LEM-GESS. By undertaking such a comprehensive analysis, we can advance our understanding of the intricate relationship between the chosen linear electric machine and the overall success of the gravity energy storage system.

To effectively implement an LEM-GESS, it is important to carefully select a linear electric machine that is well suited for long-stroke applications. Notably, linear vernier hybrid and linear flux switching machines have emerged as particularly promising configurations for this purpose [14]. These LEMs consist of compact primary components, and resilient and salient passive secondary components. This specific arrangement is advantageous for the LEM-GESS because more costly components, such as armature windings, permanent magnets (PMs), or field windings, are positioned on the short primary of the LEM.

The primary objective of this study is to conduct a comprehensive quantitative analysis of selected LEMs optimized for deployment as the primary drive unit within the LEM-GESS framework. This study thoroughly explores a detailed comparison among the consequent pole linear vernier hybrid machine (CP-LVHM), linear permanent magnet flux switching machine (LPM-FSM), and linear wound field flux switching machine (LWF-FSM) to determine the drive unit that makes the LEM-GESS the most appealing and cost-effective. A design methodology for the linear machines is proposed, and the examined parameters include the thrust, thrust ripple, normal force, power factor, efficiency, and cost.

Section II explains the LEM-GESS structure and provides a foundational understanding of its configuration. Section III explains the sizing considerations for both the machine and piston. Section IV explores the different machine topologies, and Section V details the design optimization methodologies employed. Section VI presents an in-depth analysis of the time-step finite element analysis (FEA) of the machines, and concludes with a comparative evaluation of their performance and cost. Finally, Section VII summarizes the findings of the study, draws conclusive remarks, and identifies the most promising machine configuration for optimal integration into the LEM-GESS. Through this systematic exploration, this study aims to provide valuable insights into the selection and optimization of linear electric machines for gravity energy storage systems. This research focuses solely on assessing the performance of the energy storage system when used for the primary response application with the assumption of a consistent electrical energy price and a fixed number of charge-discharge cycles per year [13]. Additionally, we presume uniformity in the shaft structure housing the LEM-GESS across all the examined drive units.

II. DESCRIPTION OF THE LEM-GESS

A linear electric machine gravity energy storage system is a type of mechanical energy storage system under the gravity storage classification [13], where a linear machine moves a piston mass up and down a shaft during the charging and discharging of electrical energy. Vertical shafts can be above ground or underground, making use of decommissioned deep mine shafts in the case of South Africa. Unlike conventional wire-rope hoisting systems, such as the gravitricity system [15], the inherently rope-less LEM-GESS operates with multiple piston masses in a single shaft. Therefore, more energy can be stored in a single shaft with the LEM-GESS compared to the gravitricity system. In addition, the use of linear machines instead of rotary machines eliminates the need for gears and other mechanical couplings, thus providing better efficiency and the required precision in dynamic systems [16].

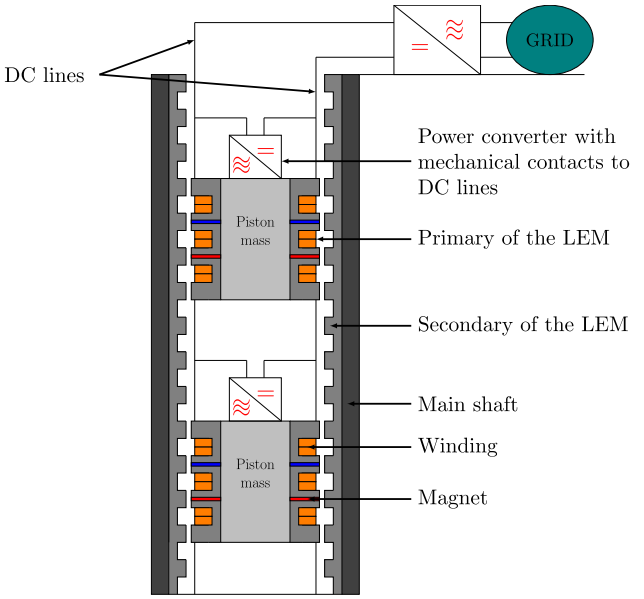

FIGURE 2. A cross-section of the LEM-GESS.

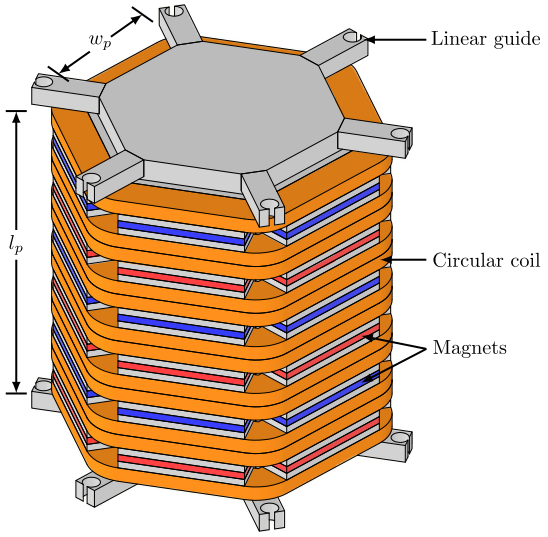

FIGURE 3. Short primary mover subsystem.

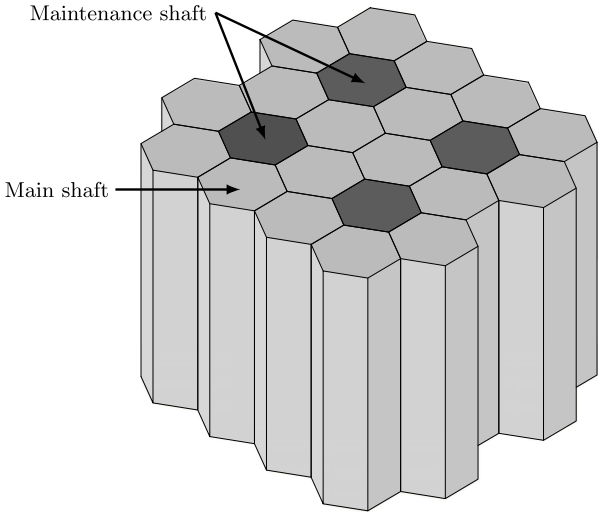

FIGURE 4. Outer view of the beehive LEM-GESS.

Fig. 2 shows a schematic of the LEM-GESS, indicating the main system components. During the charging cycle, the converter-fed LEM draws electrical power from the grid and moves the piston mass up the shaft, thereby storing the electrical energy as potential energy. During the discharging cycle, the piston mass is moved down the shaft, converting the stored potential energy to electrical energy. This energy is then supplied to the grid via a bi-directional power converter.

The LEM of a dry gravity energy storage system consists of primary or primary mover (moving) and secondary (stationary) components. To ensure a low-cost system, the secondary, as shown in Fig. 2, should be made of a low-cost material as it traverses the entire length of the shaft. A short primary mover consisting of all the active materials (windings and magnets or windings only) is suitable for long-stroke applications. The primary mover is attached to the piston mass forming primary mover subsystem. A hexagonal piston with a width w_p and height l_p is used, as shown in Fig. 3. The hexagonal design provides good space utilization and good structural strength. The LEM-GESS structure is modular thus, several shafts can be stacked to form a beehive system, as shown in Fig. 4.

III. SYSTEM SIZING

The shear stress of the machine can be used to relate the piston size to that of the machine. The sizing of the machine based on the air gap shear stress is given as follows:

$$\sigma = \frac{F}{A}, \tag{1}$$

where σ is the shear stress, F is the thrust, and A is the effective air gap area. Assuming a uniform air gap, the hexagonal piston width can be determined from [10]

$$\sigma = \frac{m(a+g)}{6w_p l_p}, \tag{2}$$

$$\sigma = \frac{\sqrt{3}}{4}\rho w_p(a+g), \tag{3}$$

where ρ is the density of the piston material, a is the acceleration of the piston mass, and g is the acceleration due to gravity. Assuming that the acceleration of the piston a is very low compared to g, (3) reduces to

$$\sigma \approx \frac{\sqrt{3}}{4}\rho w_p g. \tag{4}$$

Table 1 lists the details of the iron piston configuration and dimensions calculated based on a machine with a shear stress of approximately 35 kN/m^2 [14]. The shear stress given in (4) is independent of l_p, and if w_p is fixed, then the piston length l_p can be varied to match that of the machine by making the

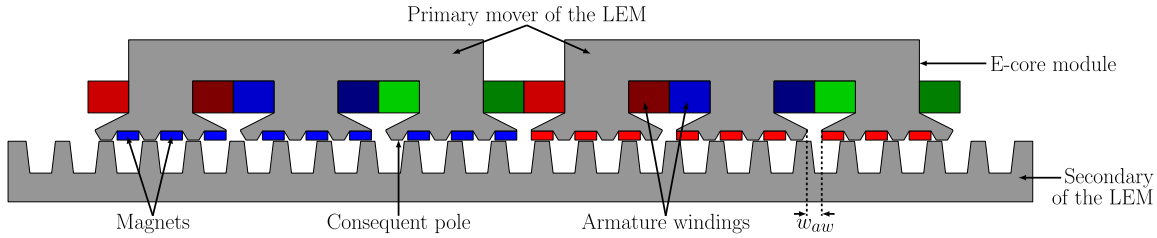

FIGURE 5. CP-LVHM structure showing main components.

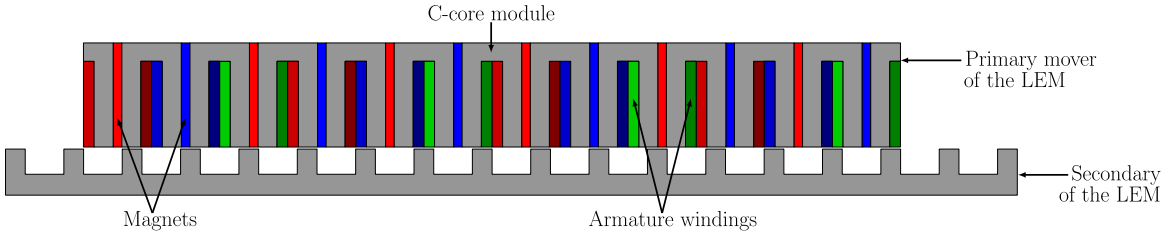

FIGURE 6. LPM-FSM structure showing main components.

TABLE 1. Iron piston specifications.

Parameter	Value
Mass (m)	50 [tons]
Density (ρ)	7850 [kg/m^3]
Shear stress (σ)	35 [kN/m^2]
w_p	1000 [mm]
Piston sides	6

piston hollow to maintain the same piston mass. The thrust required to lift the piston mass is estimated as follows:

$$Thrust = mg + ma, \tag{5}$$

$$\approx mg, \tag{6}$$

under the assumption that the acceleration a of the piston mass is very low. The acceleration can be considered as being similar to mining hoisting systems which is typically in the range of 0.5-0.75 m/s^2 [17]. Considering a hexagonal piston, the LEM must generate a thrust of approximately 84 kN per piston side to move a 50 ton piston.

IV. MACHINE TOPOLOGIES

Linear electric machines with both a field magnetomotive force (MMF) source and armature windings on the primary mover have attracted considerable attention, particularly for long-stroke applications. This is primarily attributed to the high cost of the active materials, particularly rare-earth PMs. If integrated into the elongated secondary of the LEM, this would render the machine excessively expensive. Thus, machine topologies with simple passive secondary, PM, and winding materials on a short primary mover are very attractive for long-stroke applications such as the LEM-GESS.

A consequent pole linear vernier hybrid machine (CP-LVHM) consists of a modular structure with a short primary mover made of an E-shaped iron core module having split teeth as shown in Fig. 5. Each split tooth consists of alternating consequent poles and PMs. The passive secondary is robust, with laminated salient poles. A three-phase machine is achieved by setting the distance w_{aw} between the teeth of the E-shaped iron core equal to [16]

$$w_{aw} = (n \pm 1/3)\tau_t, \tag{7}$$

where n is an integer and τ_t is the secondary tooth pitch. Sinusoidal flux linkage is achieved by placing concentrated windings on individual E-core module teeth.

According to the theory of linear vernier machines, the armature winding pole pairs are related to the number of PM pole pairs and secondary teeth by [18]

$$p_a = |n_s \pm p_{pm}|, \tag{8}$$

where n_s, p_{pm} and p_a are the number of secondary teeth, PM pole pairs, and armature winding pole pairs, respectively.

A linear permanent magnet flux switching machine (LPM-FSM) is a doubly salient machine composed of C-core modules sandwiching magnets alternating in polarity, as illustrated in Fig. 6. The magnetization of the PMs is perpendicular to the armature winding field hence, there is less demagnetization field from the armature reaction. The secondary is made of salient poles, similar to those of the CP-LVHM.

Both the CP-LVHM and LPM-FSM adopt concentrated windings featuring short-end windings. The CP-LVHM and LPM-FSM operate based on the flux modulation principle with a small primary mover position displacement, resulting in a rapid change in the flux linkage amplitude and polarity. The thrust is mainly due to the PM excitation, with the reluctance thrust being negligible.

The linear wound field flux switching machine (LWF-FSM) structure is similar to the LPM-FSM only that the PMs

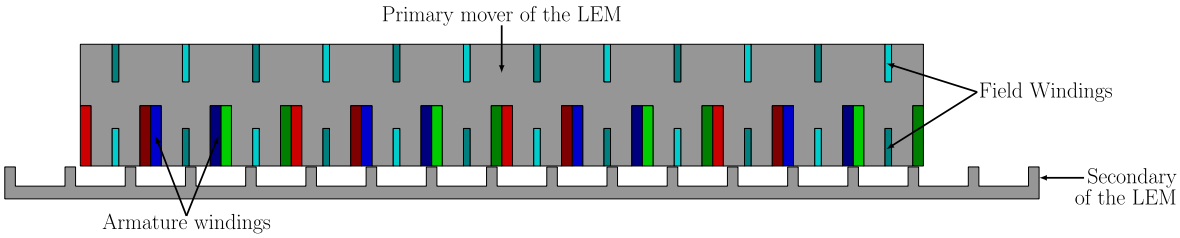

FIGURE 7. LWF-FSM with toroidal field windings (LWF-FSM TOR).

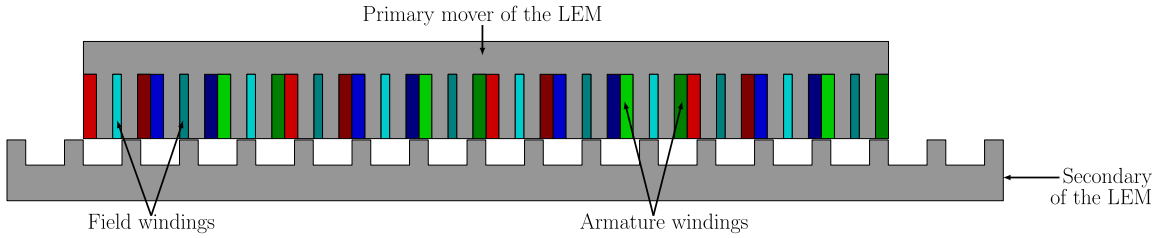

FIGURE 8. LWF-FSM with circumferential field windings (LWF-FSM CIR).

are replaced with field windings. The LWF-FSM has two configurations, toroidal and circumferential field windings, as shown in Fig. 7 and 8, respectively.

The LWF-FSM without rare-earth PM material is made of electromagnetic steel, armature windings, and DC field-excited windings, which are the main sources of the field MMF. The secondary structure is similar to that of the CP-LVHM and LPM-FSM with stacked laminated iron. The absence of PMs means that the LWF-FSM does not suffer from the risk of irreversible demagnetization, which reduces the reliability of the machine. Compared with CP-LVHM and LPM-FSM, the LWF-FSM has low force and power densities owing to excitation losses [19].

There is very little performance difference between single-layer and double-layer field winding configurations [20]. In this study, a single-layer winding configuration for the DC field windings of LWF-FSMs is considered in the analysis. In LWF-FSMs, a constant current is supplied to the field windings, which produces a constant magnetic field in the air gap. A time-variant current is fed to the armature windings, and a symmetrical sinusoidal back EMF can be obtained using a proper combination of slots and poles [21].

The operation of the machines in this study is based on the flux modulation effect. The magnetic field generated by the PMs or field windings is modulated by the salient poles of the secondary. The air gap is rich in harmonics from the modulation and these link with the armature windings to produce an effective flux linkage. The electromagnetic force is generated by several dominant harmonics of synchronized no-load air gap field harmonics and armature reaction field harmonics with the same pole pairs and speed.

The displacement of the short primary mover by a secondary tooth pitch results in a full cycle of the flux linkage. As shown in Fig. 9, a positive maximum flux linkage is attained in one phase winding with the d-axis alignment

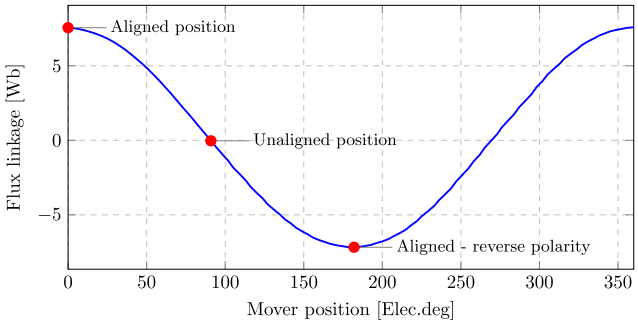

FIGURE 9. Coil flux linkage change with mover position.

occurring when the secondary and primary teeth are aligned, resulting in the minimum reluctance of the magnetic circuit. When the primary mover is displaced by $1/4\tau_t$ (unaligned position), the reluctance of the magnetic circuit is at its maximum and a minimum flux linkage is achieved. When the primary mover is displaced by $1/2\tau_t$, the polarity of the flux linkage is reversed (because the direction of the flux passing through the winding is reversed), and a negative maximum flux linkage is attained (aligned - reverse polarity).

This rapid change in the flux linkage amplitude and polarity over a small primary mover displacement leads to the generation of high thrust, even at low speeds. The relationship between the linear speed of the primary mover and the magnetic field is given by:

$$v_\phi = G_r v_t, \tag{9}$$

where v_ϕ and v_t are the speeds of the magnetic field and the primary mover, respectively, and G_r is the pole ratio.

For the flux switching machines, a 12/14 slot-pole combination is selected given the advantages of low ripple and high thrust compared to the 12/10 slot-pole combination [21].

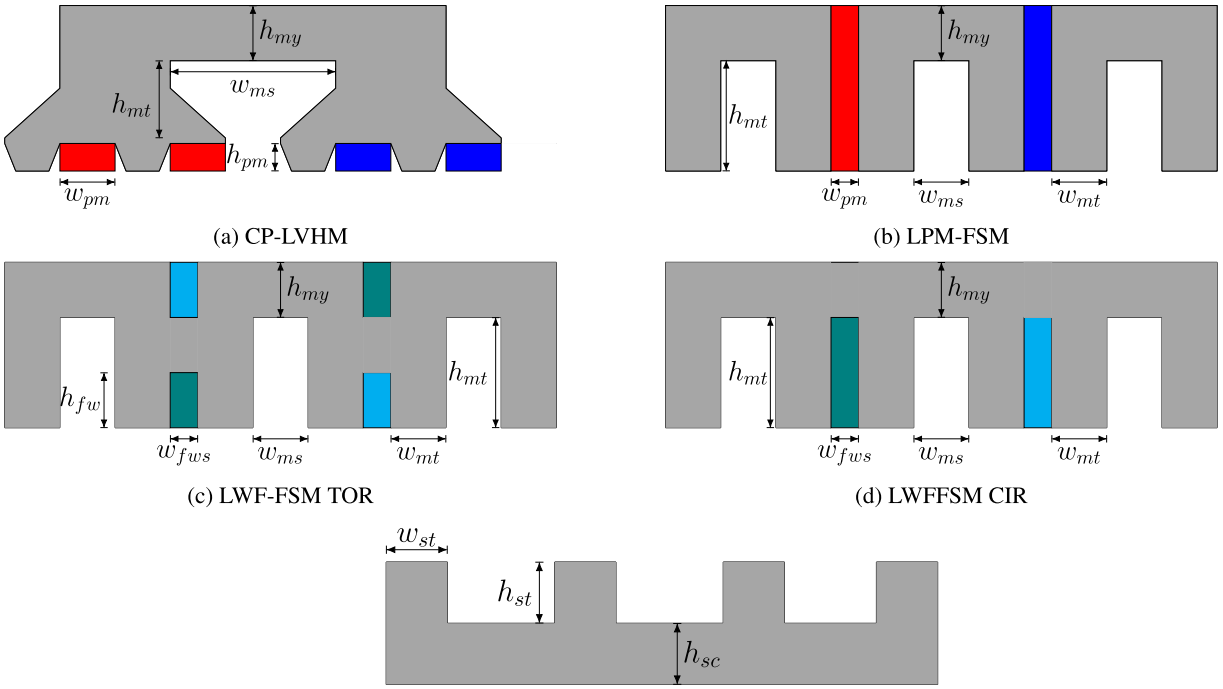

(a) CP-LVHM

(b) LPM-FSM

(c) LWF-FSM TOR

(d) LWFFSM CIR

(e) Secondary of the LEM

FIGURE 10. Geometric design optimization variables.

V. DESIGN OPTIMIZATION

Design optimization of the four machines was carried out using NSGA-II, which supports multiple objectives and multiple constraints [22]. In the optimization, the machine is analyzed using two-dimensional (2D) static FEA.

The multi-objective optimization problem is formulated as follows:

$$f(\mathrm{X}) = min\ (\mathrm{LCOS}), \tag{10}$$

where X is the geometric vector variable, whose size is the number of design variables of the machine and LCOS is the levelized cost of storage. Fig. 10 shows the geometrical variables of the machines to be optimized with the machine operating under steady-state load conditions.

The LCOS is minimized subject to the following constraints:

$$\begin{cases} J \leq 5\ \mathrm{A/mm^2} \\ \mathrm{Thrust} \geq 84\ \mathrm{kN} \\ \mathrm{Thrust\ ripple}\ < 15\% \end{cases} \tag{11}$$

The current density is limited to ensure that the winding temperature is within the set limits for continuous operation without degrading the machine performance or requiring a forced cooling system. To obtain an optimal modular machine, each side of the piston consists of three machines. Each optimal machine generates 28 kN with the three machines combined in series, generating a total of 84 kN. For all six sides of the piston, the overall thrust generated is 504 kN, the minimum required to move the 50 ton piston mass. For smooth operation and reduction of mechanical stress in the structure, thrust ripple is restricted. The stack width of the machine is constrained by the piston width (w_p) as shown in Fig. 3.

The LCOS is a cost metric that provides the overall cost of designing, constructing, and utilizing an energy storage system over the course of its useful life cycle. This financial metric indicates the average cost per MWh required for an energy storage system to deliver useful electrical energy over its lifetime, thereby balancing the overall costs associated with the system (the average energy price required to make the investment's net present value zero) [23], [24]. The LCOS is a good indicator that allows for the comparison of energy storage systems with different lifespans. The LCOS metric is of the form given in [13] as:

$$\mathrm{LCOS}\left[\frac{\mathrm{US\$}}{\mathrm{MWh}}\right] = \frac{\mathrm{CAPEX} + \mathrm{OPEX}}{\mathrm{Energy\ output}}, \tag{12}$$

where CAPEX is the capital expenditure cost and OPEX is the operation and maintenance cost of the system considering the interest rate over the lifetime of the system.

By minimizing the LCOS, the optimization essentially maximizes the power factor and efficiency of the machine while minimizing its material mass. The power factor of the machine determines the rating of the required power converter, which contributes to the CAPEX. The efficiency of the machine determines the energy output of the storage system and charging cost of the system which is part of the OPEX. A high efficiency reduces the charging cost while also increasing the energy output of the system, thus lowering

TABLE 2. Key parameters and design variables of the optimized machines.

Parameter	Unit	CP-LVHM	LPM-FSM	LWF-FSM TOR	LWF-FSM CIR
Air gap length	[mm]	2	2	2	2
AC rms current density (J_{ac})	[A/mm^2]	1.9	3.15	2.64	3.05
DC current density (J_{dc})	[A/mm^2]	-	-	2.86	3.15
Primary mover yoke height (h_{my})	[mm]	51.2	18.1	135.5	44.6
Primary mover tooth height (h_{mt})	[mm]	90.6	76.5	116.3	93.9
Width of mover tooth (w_{mt})	[mm]	149.8	25.8	49.7	36.7
Width of mover slot (w_{ms})	[mm]	77.7	25	24.8	25
Width of PM (w_{pm})	[mm]	25	7.3	-	-
Width of field winding (w_{fw})	[mm]	-	-	19.3	23.2
Height of field winding (h_{fw})	[mm]	-	-	100.4	93.9
Width of secondary tooth (w_{st})	[mm]	13.6	23.1	42.2	35.3
Height of secondary tooth (h_{st})	[mm]	31	25.4	39.6	34.9
Height of secondary core (h_{sc})	[mm]	40.9	16.9	38.6	36
Stack width (w_p)	[mm]	1 000	1 000	1 000	1 000
Mover length (l_p)	[mm]	3 078.7	3 016.5	5 166.7	4 377.6
Split ratio		0.38	0.44	0.31	0.5
Mover mass*	[kg]	2 359.8	1 456.5	8 039.7	3 368.6
Magnet mass*	[kg]	121.9	185.5	-	-
Copper mass*	[kg]	309.9	295.8	1 045.2	700.2
Secondary steel mass*	[kg/m]	403.3	191.7	398.1	364.6
Volume	[m^3]	0.5868	0.3673	1.47	0.7643
Speed	[m/s]	1	1	1	1
Frequency	[Hz]	20	13.9	8.1	9.6

* One side of the hexagonal piston

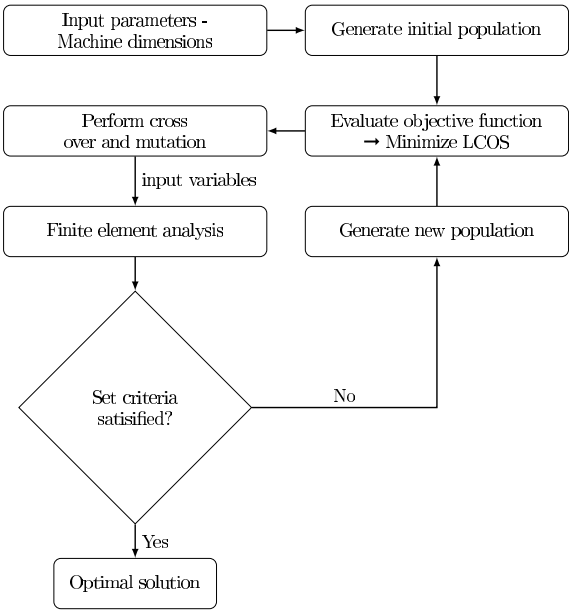

FIGURE 11. Design optimization flow chart.

the LCOS. The material mass cost and construction of the machine contribute to the CAPEX.

Fig. 11 shows a flow-chart of the machine optimization process. The NSGA-II in the VisualDOC optimization kit [25] is coupled with an external 2D static FEA package to obtain an optimal solution based on a set criterion. From the initial input parameters of the machine, a population is generated, and the input variables obtained from cross-over and mutation are used to generate a model in the 2D static FEA package. The solutions from the FEA package are analyzed using VisualDOC, considering the set constraints. When the set constraints are satisfied, an optimal solution is obtained. If the set constraints are not satisfied, then a new population for the input variables is generated and evaluated based on the objective function. This process is repeated until the optimal solution is obtained. Table 2 lists the optimal parameters for the four machines.

VI. PERFORMANCE AND COST COMPARISON

To develop a qualitative understanding of the most suitable main drive machine topology for the LEM-GESS, an electromagnetic performance comparison is conducted using 2D FEA. The electromagnetic performances of the four machines are evaluated under steady-state conditions. The end-winding inductance and resistance are calculated analytically, and their effects are included in the performance analysis. A cost analysis of each machine when used as the main drive unit of the LEM-GESS is conducted, and the LCOS is compared to reveal the most cost-effective drive technology within the set conditions.

A. THRUST CAPABILITIES AND QUALITY

All the machines are optimized to provide a thrust of approximately 84 kN per piston side. Fig. 12 shows the output thrust for all four machines with an average thrust above the required 84 kN under rated on-load conditions. It is interesting to note that the LPM-FSM achieves the required force with the lowest overall material volume. However, this does not automatically imply the least cost as the material composition is different for all four machines analyzed.

The thrust ripple effect in linear machines is undesirable because it degrades machine performance and causes vibrations which may affect the structural strength of the

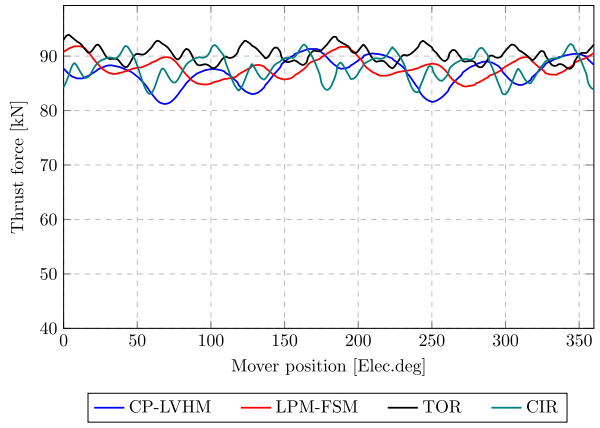

FIGURE 12. Instantaneous thrust characteristics of the machines.

shaft. The smooth operation of the machine within the shaft is desirable to ensure the integrity of the LEM-GESS housing structure. Therefore, the analysis of the thrust ripple is important, particularly for such a system with high forces throughout the shaft of the LEM-GESS. The CP-LVHM has the highest ripple of 14.7% and the LWF-FSM TOR has the least ripple of 7.9%. The LPM-FSM and LWF-FSM CIR have ripples of 8.4% and 10.5%, respectively.

Step-positioning [26] and the use of end-teeth [27] are techniques that can be used to reduce the thrust ripple in linear vernier machines and linear flux switching machines to improve the thrust quality, as shown in Figs. 13 and 14, respectively. However, the thrust ripple reduction techniques can also result in a reduction in the thrust output thus, care must be taken to ensure that the resultant thrust does not fall below the required thrust.

Both ripple-reduction techniques are applied to all machines however, only the best for each machine is discussed further. By step-positioning the three CP-LVHM machines on one side of the piston, as shown in Fig. 13, a reduction in the thrust ripple is observed. In Fig. 15, we see that a lower thrust ripple of 8.7% can be achieved at $d_s = 48$ mm with the minimum thrust requirement.

The use of additional end-teeth for the LPM-FSM, as shown in Fig. 14, is an effective technique that reduces the thrust ripple from 8.4% to 6.8%. The LWF-FSMs' show a reduction in thrust ripple by step-positioning. The thrust ripple of the LWF-FSM TOR is reduced to 5.8% and that of the LWF-FSM CIR is reduced to 6.3% as shown in Fig. 16 and 17, respectively. Fig. 18 shows the thrust ripple characteristics of the machines before and after the ripple-reduction techniques are applied.

The estimated no-load back-EMF is analyzed to verify the principle of machine operation. Fig. 19 shows the no-load back-EMF of the analyzed machines at 1 m/s. The sinusoidal three-phase back-EMF waveforms of the machines positively impact the converter performance, resulting in a better overall system efficiency.

The detent force (no-load force), which is a major cause of thrust ripple, is a result of the slot-effects, which cause variations in the air gap flux density and end-effects owing to the finite length of the primary mover. Fig. 20 shows the detent force of the machines. It is observed that the CP-LVHM had the largest peak-to-peak detent force, which has a direct impact on the thrust quality inform of high thrust ripple. The LPM-FSM has the lowest detent force, resulting in a much smoother output thrust, particularly at low speeds.

The normal force component of linear machines is of keen interest as it determines the rigidity and robustness of the shaft housing structure of the LEM-GESS in order to withstand the attraction forces. A lower normal/attraction force is desirable because it results in a less expensive shaft housing structure.

Fig. 21 shows the normal force on one side of the linear machines between the primary mover and secondary of the LEM. The LWF-FSM TOR has the highest normal force of 800.8 kN with a ripple of 6.1% followed by the LWF-FSM CIR with a normal average force of 793.7 kN with 4.2% ripple. The LPM-FSM has a normal average force of 576.9 kN with the lowest ripple of 2.9%. The CP-LVHM has the lowest normal average force of 320 kN however, it has the highest ripple of 10.2%, which can cause undesirable vibrations in the structure. This creates a need for a much stiffer and more secure structure.

B. EFFICIENCY APPROXIMATION

The efficiency of the machines is estimated based on (13)

$$\eta = \frac{P_{out}}{P_{out} + P_{cu} + P_{iron}}, \tag{13}$$

where P_{out}, P_{cu} and P_{iron} are the power output, copper loss, and iron loss respectively. The CP-LVHM has the highest efficiency of 94.7% whereas the LWF-FSM TOR has the lowest efficiency of 72.2%. The LPM-FSM and LWF-FSM CIR have efficiencies of 91.3% and 77.0%, respectively.

The CP-LVHM with a low current density and larger copper area has lower copper losses than the other machines. The CP-LVHM has a long flux path and higher frequency, resulting in more core losses compared with the LPM-FSM and LWF-FSMs.

C. POWER FACTOR CHARACTERISTICS

Based on the phasor diagram in Fig. 22, the power factor of the machines can be estimated using a simplified equation, with the voltage drop across the phase resistance ignored, as in [28].

$$\begin{aligned} \cos\phi &= \frac{E_o}{V_o}, \\ &= \frac{E_o}{\sqrt{E_o^2 + (X_q I_q)^2}}, \\ &= \frac{1}{\sqrt{1 + (\frac{X_q I_q}{E_o})^2}}, \end{aligned} \tag{14}$$

where E_o, X_q, I_q are the induced voltage, synchronous reactance, and q-axis current [29]. V_o is the resultant terminal

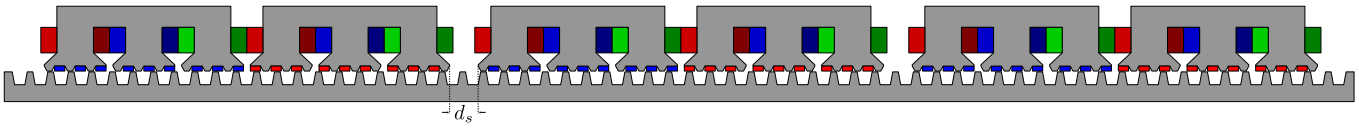

FIGURE 13. Step positioned CP-LVHM.

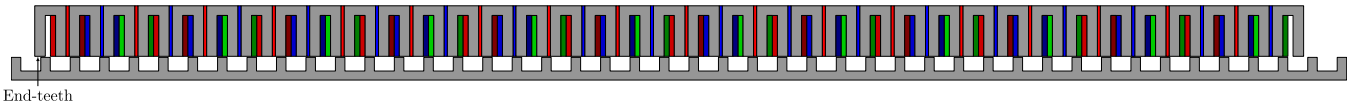

FIGURE 14. LPM-FSM with end-teeth.

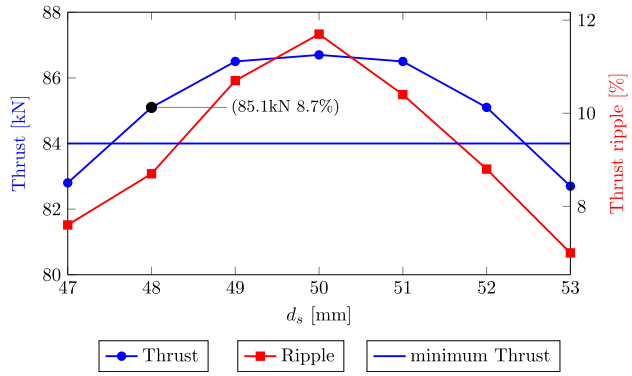

FIGURE 15. Thrust ripple variation with d_s: CP-LVHM.

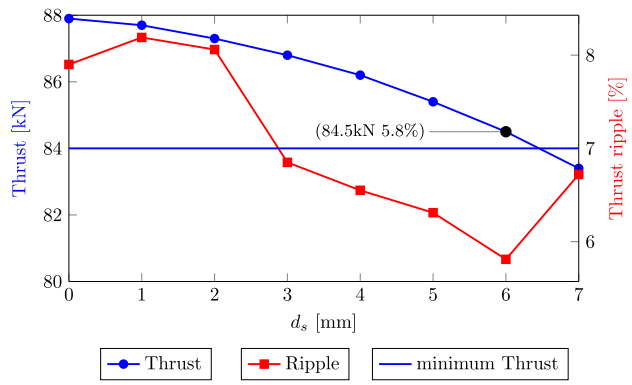

FIGURE 16. Thrust ripple variation with d_s: LWF-FSM TOR.

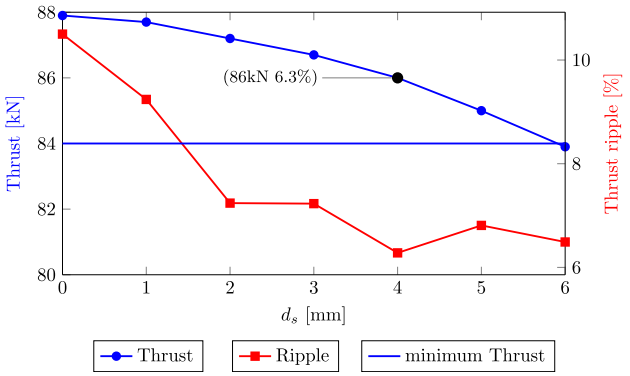

FIGURE 17. Thrust ripple variation with d_s: LWF-FSM CIR.

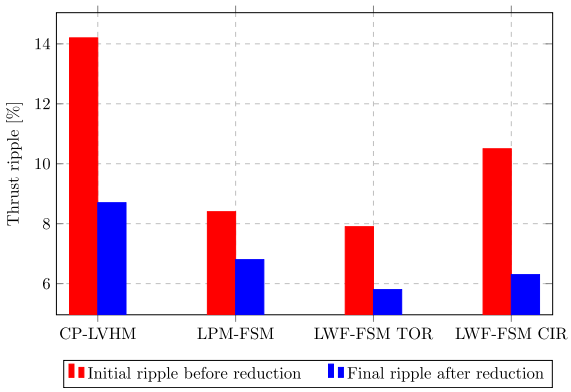

FIGURE 18. Thrust ripple characteristics of the machines.

voltage. The CP-LVHM has the lowest power factor because of its high inductance, as shown in Fig. 23, which is typical of vernier machines [16]. A low power factor results in higher costs associated with the power converters. From the electromagnetic analysis, the CP-LVHM, LPM-FSM, LWF-FSM TOR, and LWF-FSM CIR have power factors of 0.43, 0.7, 0.49, and 0.6, respectively.

D. SYSTEM MASS AND COST

Assuming a similar shaft housing structure, the cost contribution of the LEM-GESS shaft housing structure and excavation cost of the shaft (considering the underground system) to the CAPEX is the same for all four machines. A 20 MW/10 MWh energy storage system for primary frequency response application is considered with an effective shaft depth of 1000 m, 74 hexagonal piston iron masses, and structural and excavation costs, as in [13].

The costs of the materials for the machines are listed in Table 3. Table 4 lists the breakdown of the costs per material of different machines for a LEM drive unit. The CP-LVHM has the highest secondary steel cost, which is approximately twice that of the LPM-FSM with the lowest cost. Although the LPM-FSM has a high magnet cost of approximately 35%

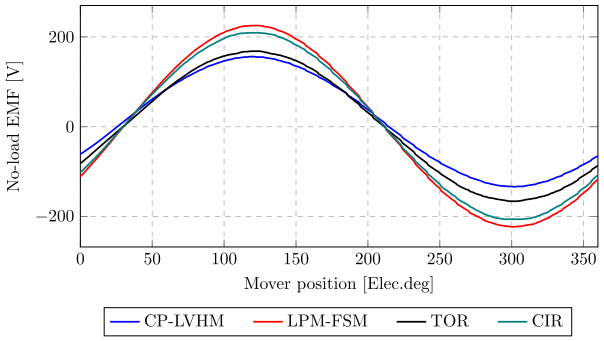

FIGURE 19. No-load back-EMF characteristics of the machines.

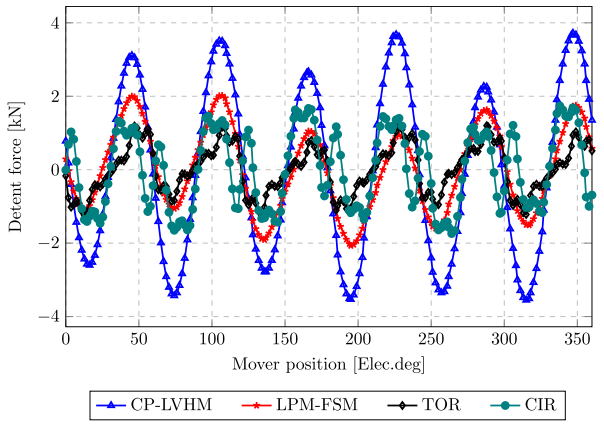

FIGURE 20. Detent force characteristics of the machines.

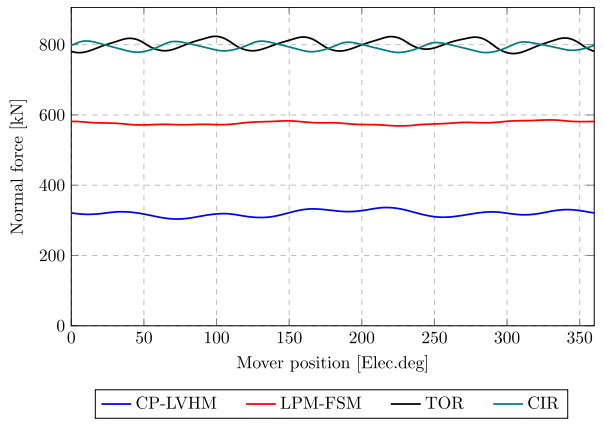

FIGURE 21. Normal force characteristics of the machines.

more than the CP-LVHM, the low secondary cost makes the LPM-FSM have a relatively low total machine cost compared with the CP-LVHM for the entire shaft depth. Overall, for the 20 MW/10 MWh LEM-GESS with an effective shaft depth of 1000 m, the LWF-FSM CIR has the lowest machine cost, followed by the LPM-FSM, CP-LVHM, and LWF-FSM TOR with the highest total machine cost.

Referring to (12), the LPM-FSM emerges as the most economical machine when employed as the main drive technology, resulting in an LCOS of 166.9 $/MWh for the

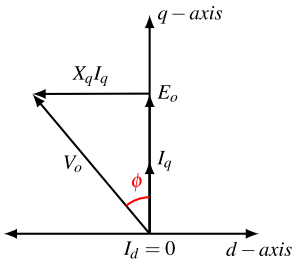

FIGURE 22. Phasor diagram.

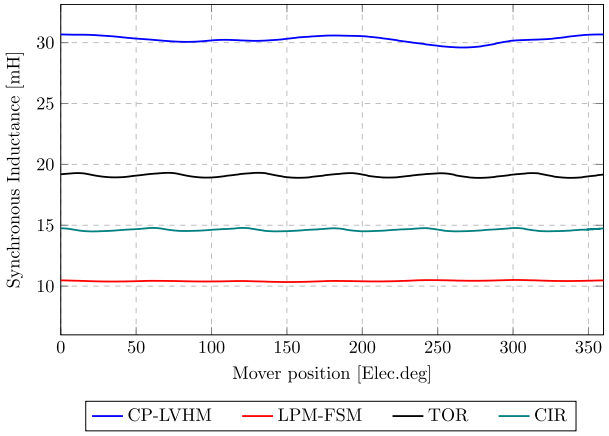

FIGURE 23. Synchronous inductance.

TABLE 3. Material costs [30].

Material	Cost
Silicon steel [$/kg]	2
Copper [$/kg]	8
Magnet [$/kg]	100

LEM-GESS. Following closely is the CP-LVHM, yielding an LCOS of 172.3 $/MWh, and subsequently, the LWF-FSM CIR yielding an LCOS of 215.6 $/MWh for the LEM-GESS. The LWF-FSM TOR, on the other hand, proves to be the least economically efficient, resulting in an LCOS of 257.9 $/MWh for the LEM-GESS.

In the study conducted by Mugyema et al. [13], a comprehensive LCOS comparison was performed for an LEM-GESS, flywheel, lithium-ion battery, vanadium redox flow battery, and lead-acid battery energy storage systems, all configured for a 20 MW/10 MWh storage capacity. Among the currently existing flywheel and battery technologies, the results indicated that the flywheel energy storage system is the most favorable option, boasting an LCOS of 185.5 $/MWh. From the analysis of the machines for LEM-GESS, it becomes evident that PM-based machine options render the LEM-GESS highly competitive compared to non-PM-based alternatives, particularly when used for primary response.

TABLE 4. Machine costs of a LEM drive system.

	Unit	CP-LVHM	LPM-FSM	TOR	CIR
Secondary steel	[$/m]	4 838	2 300	4 777	4 375
Primary mover	[$]	118 736	145 741	146 645	74 030
Primary steel	[$]	28 317	17 478	95 474	40 123
Copper	[$]	14 875	14 198	50 169	33 109
Magnet	[$]	73 140	111 300	-	-
Total cost*	[million $]	15.1	13.8	17.7	11.7

* Total cost for 74 pistons and effective shaft depth of 1000 m

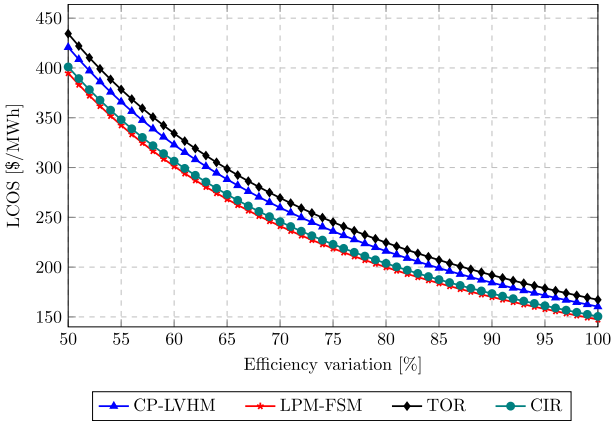

FIGURE 24. Sensitivity analysis of the efficiency on LCOS.

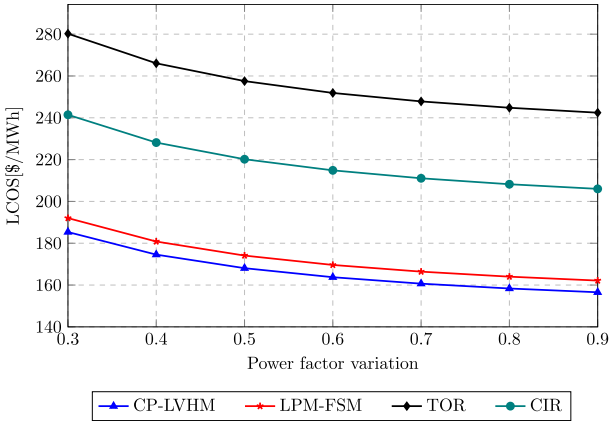

FIGURE 26. Sensitivity analysis of the power factor on LCOS.

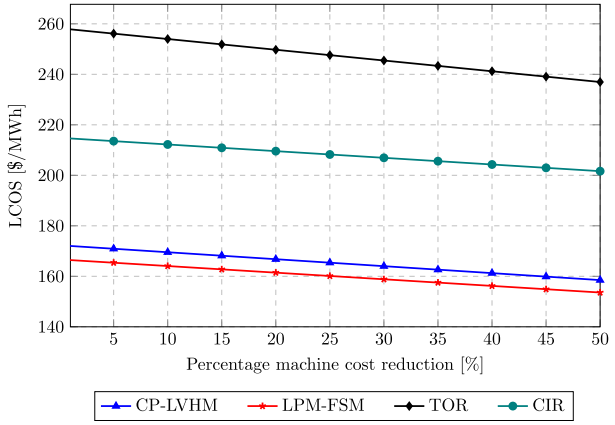

FIGURE 25. Sensitivity analysis of the machine cost on LCOS.

The cost analysis highlights the significant role of system efficiency in reducing the overall LCOS for the LEM-GESS. This is evident with the LWF-FSM CIR, which boasts approximately 15% lower machine cost compared to the LPM-FSM. However, it also experiences a 15.7% lower efficiency, leading to the LEM-GESS having an LCOS that is 29.2% higher than when utilizing an LPM-FSM. The sensitivity of efficiency on the LCOS is shown in Fig. 24. We observe that a 1% to 2% increase in efficiency leads to a reduction in the LCOS by approximately 1.3% to 2.9%. A high efficiency can potentially make the system cost-effective.

Efficiency has a significant impact on the LCOS, followed by the machine cost. Fig. 25 shows the change in the LCOS as the machine cost decreases. The machine cost variation has a linear relationship with LCOS. We observe that a 10% decrease in the total machine cost leads to a 1.2% to 1.6% decrease in the LCOS.

The LPM-FSM has the highest power factor of 0.7 implying lower costs associated with the power converter compared with the CP-LVHM and LWF-FSMs. For almost similar voltages, the CP-LVHM and LWF-FSMs have a higher current rating compared to the LPM-FSM, consequently increasing the losses associated with the power converter, which would further reduce the overall system efficiency [31].

Fig. 26 shows the sensitivity of the power factor to the LCOS. We observe that the power factor has a non-linear relationship with the LCOS. For power factor values below 0.5, there is a much greater decrease in the LCOS as the power factor increases. Above a power factor of 0.7, the effect on the LCOS becomes relatively small. For example, a 10% increase in the power factor of the CP-LVHM from 0.43 to 0.473 causes a 1.6% decrease in the LCOS. Above a power factor of 0.7, the LCOS reduction is approximately 1% for a 10% increase in power factor.

It's worth mentioning that while using LWF-FSMs lead to a relatively higher LCOS for the LEM-GESS compared to when it utilizes linear PM machine options, using non-PM linear machines has certain advantages such as ease of manufacturing, assembly, and maintenance. The LWF-FSM CIR is the best performing non-PM machine option. Table 5 presents an overview of the electromagnetic performance of

TABLE 5. Main predicated properties of the analyzed machines.

Parameter	CP-LVHM	LPM-FSM	TOR	CIR
Turns per phase	36	84	72	84
Rated voltage (rms) [V]	224.1	223.1	216.2	219.5
Rated current (rms) [A]	306.6	206.9	305.1	245
DC field current [A]	-	-	589.3	667.3
Thrust [kN]	85.5	87.8	87.9	87.9
Thrust ripple [%]	8.7	6.8	5.8	6.3
P_{out} [kW]	83.5	87.1	82.8	84.5
P_{cu} [kW]	2.7	6.9	30.2	23.7
P_{iron} [kW]	2	1.3	1.7	1.5
Power factor	0.43	0.7	0.49	0.6
Efficiency [%]	94.7	91.3	72.2	77.0
LCOS [$/MWh]	172.3	166.9	257.9	215.6

the linear machines and the LCOS of the LEM-GESS across the four different linear machine configurations.

VII. CONCLUSION

Energy storage systems present a promising solution for effectively integrating renewable energy sources into the power grid. They address the intermittency and variability inherent in renewables, thereby boosting system resilience and grid stability. Among these systems, the recently proposed LEM-GESS stands out for its versatility, scalability, and long lifespan. However, realizing the potential of LEM-GESS requires the development of specific linear drive topologies and designs tailored precisely to its unique requirements.

This study has focused on exploring linear drive machines specifically tailored for LEM-GESS. These machines underwent optimization, after which their performance was analyzed in the context of serving as the primary drive technology in LEM-GESS for primary response application. A comparison of the performance and cost of the LEM-GESS using different drive technologies revealed the following:

- The LPM-FSM is the most cost-competitive machine when used as the main drive unit of the LEM-GESS, resulting in an LCOS of 166.9 $/MWh for the LEM-GESS.
- The LPM-FSM with an 81% higher normal/attraction force in than the CP-LVHM would require a more rigid and secure structure, increasing the costs associated with the shaft housing structure. The LWF-FSMs has the highest attraction forces approximately 2.5 times that of the CP-LVHM.
- Sensitivity analysis reveales that the efficiency of the machines has a significant impact on the LCOS. For example, a 1% increase in the efficiency of the LPM-FSM would lead to a 1.6% decrease in the LCOS to 164.2 $/MWh. High efficiency machines result in LEM-GESS being very cost-competitive.
- The cost of the machine has a lower effect on the LCOS than the efficiency, as observed from the sensitivity analysis. The power factor has the least effect on the overall LCOS.
- The LWF-FSM CIR is the most competitive non-PM option and offers unique advantages as a drive technology. In comparison to the second-best PM option, that is, the CP-LVHM, the LWF-FSM CIR has a low machine cost and better power factor however, it has a lower efficiency (18.7% lower), resulting in an LCOS that is approximately 29% higher than that of the CP-LVHM.
- Although not as appealing as their counterparts in terms of cost, non-PM machines have unique advantages, including ease of manufacturing, assembly, and maintenance. Non-PM machine options do not suffer from irreversible demagnetization, resulting in better reliability.

The best PM machine option in terms of the LCOS for the LEM-GESS is the LPM-FSM, and the best non-PM machine option is the LWF-FSM CIR resulting in an LEM-GESS with an LCOS that is 25% higher than when using a LPM-FSM as the main drive technology.

The LEM-GESS using different drive technologies has been discussed revealing its feasibility and viability as a potential energy storage solution. Future studies could focus on the practical implementation of the LEM-GESS with the most suitable drive unit. This is likely to provide more insight into other dynamic issues related to the linear drive system and the shaft housing structure.

REFERENCES

[1] J. Mitali, S. Dhinakaran, and A. A. Mohamad, "Energy storage systems: A review," *Energy Storage Saving*, vol. 1, no. 3, pp. 166–216, Sep. 2022.

[2] T. S. Le, T. N. Nguyen, D.-K. Bui, and T. D. Ngo, "Optimal sizing of renewable energy storage: A techno-economic analysis of hydrogen, battery and hybrid systems considering degradation and seasonal storage," *Appl. Energy*, vol. 336, Apr. 2023, Art. no. 120817.

[3] X. Li and A. Palazzolo, "A review of flywheel energy storage systems: State of the art and opportunities," *J. Energy Storage*, vol. 46, Feb. 2022, Art. no. 103576.

[4] M. Auguadra, D. Ribó-Pérez, and T. Gómez-Navarro, "Planning the deployment of energy storage systems to integrate high shares of renewables: The Spain case study," *Energy*, vol. 264, Feb. 2023, Art. no. 126275.

[5] (2023). *Enewables 2023: Analysis and Forecast To 2028*. [Online]. Available: https://www.iea.org/reports/renewables-2023

[6] S. Zhang, Y. Li, E. Du, C. Fan, Z. Wu, Y. Yao, L. Liu, and N. Zhang, "A review and outlook on cloud energy storage: An aggregated and shared utilizing method of energy storage system," *Renew. Sustain. Energy Rev.*, vol. 185, Oct. 2023, Art. no. 113606.

[7] A. G. Olabi, "Renewable energy and energy storage systems," *Energy*, vol. 136, pp. 1–6, Oct. 2017.

[8] W. Wang, B. Yuan, Q. Sun, and R. Wennersten, "Application of energy storage in integrated energy systems—A solution to fluctuation and uncertainty of renewable energy," *J. Energy Storage*, vol. 52, Aug. 2022, Art. no. 104812.

[9] T. M. Letcher, *Storing Energy: With Special Reference to Renewable Energy Sources*. Amsterdam, The Netherlands: Elsevier, 2022.

[10] C. D. Botha and M. J. Kamper, "Capability study of dry gravity energy storage," *J. Energy Storage*, vol. 23, pp. 159–174, Jun. 2019.

[11] C. D. Botha, M. J. Kamper, and R.-J. Wang, "Design optimisation and cost analysis of linear Vernier electric machine-based gravity energy storage systems," *J. Energy Storage*, vol. 44, Dec. 2021, Art. no. 103397.

[12] O. Schmidt, S. Melchior, A. Hawkes, and I. Staffell, "Projecting the future levelized cost of electricity storage technologies," *Joule*, vol. 3, no. 1, pp. 81–100, Jan. 2019.

[13] M. Mugyema, C. D. Botha, M. J. Kamper, R.-J. Wang, and A. B. Sebitosi, "Levelised cost of storage comparison of energy storage systems for use in primary response application," *J. Energy Storage*, vol. 59, Mar. 2023, Art. no. 106573.
[14] I. Eguren, G. Almandoz, A. Egea, G. Ugalde, and A. J. Escalada, "Linear machines for long stroke applications—A review," *IEEE Access*, vol. 8, pp. 3960–3979, 2020.
[15] (2023). *Gravitricity*. [Online]. Available: https://www.gravitricity.com/technology/
[16] Y. Du, M. Cheng, K. T. Chau, X. Liu, F. Xiao, W. Zhao, K. Shi, and L. Mo, "Comparison of linear primary permanent magnet Vernier machine and linear Vernier hybrid machine," *IEEE Trans. Magn.*, vol. 50, no. 11, pp. 1–4, Nov. 2014.
[17] T. Mushiri, M. Jirivengwa, and C. Mbohwa, "Design of a hoisting system for a small scale mine," *Proc. Manuf.*, vol. 8, pp. 738–745, Jan. 2017.
[18] H. Chen, A. M. EL-Refaie, and N. A. O. Demerdash, "Flux-switching permanent magnet machines: A review of opportunities and challenges—Part I: Fundamentals and topologies," *IEEE Trans. Energy Convers.*, vol. 35, no. 2, pp. 684–698, Jun. 2020.
[19] W. Jiang, W. Huang, X. Lin, Y. Zhao, and S. Zhu, "Analysis of rotor poles and armature winding configurations combinations of wound field flux switching machines," *IEEE Trans. Ind. Electron.*, vol. 68, no. 9, pp. 7838–7849, Sep. 2021.
[20] G. Zhao, W. Hua, and J. Qi, "Comparative study of wound-field flux-switching machines and switched reluctance machines," *IEEE Trans. Ind. Appl.*, vol. 55, no. 3, pp. 2581–2591, May 2019.
[21] J. T. Chen and Z. Q. Zhu, "Winding configurations and optimal stator and rotor pole combination of flux-switching PM brushless AC machines," *IEEE Trans. Energy Convers.*, vol. 25, no. 2, pp. 293–302, Jun. 2010.
[22] K. Deb, A. Pratap, S. Agarwal, and T. Meyarivan, "A fast and elitist multiobjective genetic algorithm: NSGA-II," *IEEE Trans. Evol. Comput.*, vol. 6, no. 2, pp. 182–197, Apr. 2002.
[23] V. Jülch, "Comparison of electricity storage options using levelized cost of storage (LCOS) method," *Appl. Energy*, vol. 183, pp. 1594–1606, Dec. 2016.
[24] Y. Amry, E. Elbouchikhi, F. Le Gall, M. Ghogho, and S. El Hani, "Optimal sizing and energy management strategy for EV workplace charging station considering PV and flywheel energy storage system," *J. Energy Storage*, vol. 62, Jun. 2023, Art. no. 106937.
[25] (2023). *Vanderplaats Research and Development, Inc*. [Online]. Available: https://www.vrand.com/products/visualdoc/
[26] I. Boldea, *Linear Electric Machines, Drives, and MAGLEVs Handbook*. Boca Raton, FL, USA: CRC Press, 2017.
[27] I. Eguren, G. Almandoz, A. Egea, S. Zarate, and A. Urdangarin, "Thrust ripple reduction in linear switched-flux machines via additional pole optimisation," *IEEE Trans. Energy Convers.*, vol. 37, no. 3, pp. 1655–1665, Sep. 2022.
[28] D. Li, R. Qu, and T. A. Lipo, "High-power-factor Vernier permanent-magnet machines," *IEEE Trans. Ind. Appl.*, vol. 50, no. 6, pp. 3664–3674, Nov. 2014.
[29] T. W. Ching, K. T. Chau, and W. Li, "Power factor improvement of a linear Vernier permanent-magnet machine using auxiliary DC field excitation," *IEEE Trans. Magn.*, vol. 52, no. 7, pp. 1–4, Jul. 2016.
[30] (2023). *Tradingeconomics*. [Online]. Available: https://tradingeconomics.com/
[31] A. Anthon, Z. Zhang, M. A. E. Andersen, D. G. Holmes, B. McGrath, and C. A. Teixeira, "Comparative evaluation of the loss and thermal performance of advanced three-level inverter topologies," *IEEE Trans. Ind. Appl.*, vol. 53, no. 2, pp. 1381–1389, Mar. 2017.

MORRIS MUGYEMA (Graduate Student Member, IEEE) received the B.Sc. (Eng.) degree from Makerere University, Uganda, in 2015, and the M.Sc. (Eng.) degree from Addis Ababa University, Ethiopia, in 2019. He is currently pursuing the Ph.D. degree with the Department of Electrical and Electronic Engineering, Stellenbosch University, South Africa. His current research interests include the design and evaluation of electric machines for renewable energy and energy storage application.

MAARTEN J. KAMPER (Senior Member, IEEE) received the M.Sc. (Eng.) and Ph.D. (Eng.) degrees from Stellenbosch University, South Africa, in 1987 and 1996, respectively. In 1989, he joined as an Academic Staff with the Department of Electrical and Electronic Engineering, Stellenbosch University, where he is currently a Distinguished Professor in electrical machines and drives. His research interests include computer-aided design and the control of reluctance, permanent magnet, and induction electrical machine drives, with applications in electric transportation and renewable energy. He is a South African National Research Foundation-rated Scientist and a registered Professional Engineer in South Africa.

RONG-JIE WANG (Senior Member, IEEE) received the M.Sc. (Eng.) degree in electrical engineering from the University of Cape Town, South Africa, in 1998, and the Ph.D. degree in electrical engineering from Stellenbosch University, South Africa, in 2003. He is currently a Professor with the Department of Electrical and Electronic Engineering, Stellenbosch University. His research interests include the novel topologies of permanent magnet machines, the computer-aided design and optimization of electrical machines, cooling design and analysis, and renewable energy systems. He is a South African National Research Foundation-rated Researcher and a registered Professional Engineer in South Africa.

BEN A. SEBITOSI (Senior Member, IEEE) received the Ph.D. degree in technology transfer on the application of advanced automotive technologies to rural electrification from the University of Cape Town, in 2005. He is currently a multidisciplinary emeritus Professor in energy with the Centre for Renewable and Sustainable Studies, Stellenbosch University. He is an Alumnus of the King's College, Budo, the University of Nairobi, and the University of Cape Town. Prior to joining academia, he had over 15 years industrial engineering background, he has been registered as a Chartered Engineer with the Engineering Council of the U.K., since 2003, and the Engineers Registration Board of Kenya, since 1987. He is evaluated as a C2-category established Researcher by the National Research Fund of South Africa. He was a recipient of the Stellenbosch University Vice Chancellor's Award, in 2010. His field of specialty is applied alternative energy systems modeling, rational use of energy, and energy policy and climate resilience. His Ph.D. degree was nominated for Joseph Arenow Best Ph.D. Award. Among his highlights, he has been a lead Consultant for a World Bank sponsored drafting of the Rwanda government energy policy and strategy, a Lead Coordinator for energy curriculum development for the Pan African University Committee Member, and a member of International Council for Science (ICSU) Task Team on energy-saving transport in sub-Saharan Africa, since 2008. He has supervised over 40 master's and P.D. students (in energy engineering and policy) and he published over 70 articles in high impact international journals. He holds a South African patent for solar day lighting.